IEEE Access
Multidisciplinary ⋮ Rapid Review ⋮ Open Access Journal

Received November 5, 2020, accepted November 17, 2020, date of publication November 25, 2020, date of current version December 10, 2020.

Digital Object Identifier 10.1109/ACCESS.2020.3040514

Evaluating Effect of Blanket Jamming on Radar Via Robust Time-Frequency Analysis and Peak to Average Power Ratio

TINGPENG LI[1,2], ZELONG WANG[2], AND JIYING LIU[2]
[1]State Key Laboratory of Complex Electromagnetic Environment Effects on Electronics and Information System, Luoyang 471003, China
[2]College of Liberal Arts and Sciences, National University of Defense Technology, Changsha 410073, China

Corresponding author: Zelong Wang (zelong_wang@163.com)

This work was supported in part by the State Key Laboratory of Complex Electromagnetic Environment Effects on Electronics and Information System Grants under Grant CEMEE2020Z0201B, in part by the National Key Research and Development Program of China under Grant 2017YFB0502703, and in part by the National Natural Science Foundation of China under Grant 61671015.

ABSTRACT Evaluating the effect of blanket jamming is at the core of performance analysis and jamming/anti-jamming design for radar. Restricted to diverse jamming types and radar's applications, it is challenging to put forward a unified framework for quantitative evaluation. To address this issue, we come up with a composite evaluation by combining the robust time-frequency analysis (RTFA) and peak to average power ratio (PAPR). In term of signal-level evaluation, RTFA is exploited to analyze the echoes directly, providing the time-frequency (TF) spectrum for calculating two-dimensional image entropy. For system/application-level evaluation, we derive the variation of signal to jamming ratio (SJR) in radar processing chain, and thus define the PAPR to associate SJR with target detection, a type of common and fundamental application that usually affects the other subsequent ones. To refine composite evaluation, we modify the traditional RTFA by leveraging joint sparse model with convolution framelets to improve TF concentration and to avoid the crossing terms; meanwhile, we derive the quantitative relationship between SJR and detection probability, leading to theoretical guarantee of PAPR for evaluation. Finally, the feasibility and the superiority of the proposed evaluation approach are validated in numerical experiments.

INDEX TERMS Effect evaluation, robust time-frequency analysis, peak to average power ratio, composite evaluation, convolution framework.

I. INTRODUCTION

Evaluating the effect of jamming on radar, i.e., exploring evaluation indices to quantitatively assess the performance of radar in complex electromagnetic environment [1]–[3], is central to performance analysis and jamming/anti-jamming design for radar systems. It is well-known that electromagnetic jamming widely exists and has remarkable influence on radar systems, including changing the echo waveforms, decreasing the signal to noise rate (SNR) of the receiver, misdirecting the radar antenna, and so on. When the jamming is targetedly designed, the performance of radar would become worse [4]. For this reason, it is desirable to perform accurate and fast analysis on the variation of radar performance under different jamming types and parameters via effect evaluation of jamming. What's more, jamming/anti-jamming design [5], [6] greatly depends on the recognition of jamming types, the estimation of jamming parameters, and even the recovery of original jamming signals, which is also closely related to effect evaluation of jamming on radar.

Evaluating the effect of jamming on radar is challenging, although it has been studied from theories to practical applications during the past several decades [7], [8]. To begin with, there are various jamming types with different parameters. For instance, the passive jamming and the active jamming [9] are two major types, while the later contains diverse blanket jamming types, such as frequency-modulation (FM) noise, amplitude-modulation (AM) noise, phase-modulation (PM) noise, and radio frequency (RF) noise. Another issue for evaluation comes from the complex processing chain of radar system as well as its numerous applications. This chain refers to lots of processing steps, e.g., digital/analog filtering, intermediate frequency and down-converting (IFDC), matched filtering, moving target identification (MTI), etc. [10], [11], and

The associate editor coordinating the review of this manuscript and approving it for publication was Prakasam Periasamy.

the applications include target detection, tracking, recognition and so on [12], [13]. For these reasons, to our best knowledge, there is no efficient and unified evaluation framework to explore the general rules on effect of jamming on radar. It is worth noting that the blanket jamming has attracted more and more attentions for its great degree of flexibility [14] and that pulse Doppler (PD) radar plays a leading role in practical applications [15], so the evaluation can be limited to blanket jamming and PD radar. Despite this constraint, the difficulty in evaluation still remains.

To address these issues, the evaluation methods with different indices have been proposed in the viewpoint of signal (i.e. signal-level evaluation), which directly focus on radar echoes or their transforms. For instance, wavelets weight correlation coefficient of signals has been exploited to demonstrate the jamming effectiveness for moving tracked vehicles [16]. Indeed, many popular physical quantities, such as bandwidth, SNR, SJR, entropy, etc., are always used to measure the quality of signals with jamming [17], [18]. These signal-level evaluation methods, however, quickly become impractical as they often must require distinct signal models and algorithms or rely on good observation conditions (e.g. high SNR or complete data). Although feature extraction and recognition of jamming types [19], [20] offers new insights to effect evaluation by calculating entropy feature to restrain AM jamming [21] or extracting spectrum feature to recognize deception jamming [22], it still comes with no guarantee of feature precision due to extreme jamming environment (e.g. jamming with high intensity or unknown types). Although signal-level evaluation methods are explicit and simple, they still fail to have a direct link to practical applications of radar systems, resulting in the lack of pertinence to specific applications or systems.

Another type of popular approaches for effect evaluation is in the sense of systems and applications (i.e. system/application-level evaluation), where concrete systems or applications, such as moving target detection (MTD), constant false-alarm rate (CFAR) detection, target tracking correlation, and so on, are usually taken into account. Their success comes from the fact that the variation of the indices of the systems or applications can present the behavior of jamming. They, however, rely on numerous simulations or experiments with various parameters or conditions [10], and thus have high cost of time, computation and software/hardware. We refer to [7], [8], [11] for more details. Even if their pertinences to specific systems or applications have been enhanced greatly, there are few opportunities to extend or transfer their achievements to other cases. This limitation arises from the fact that they seldom put emphasis on jamming mechanism and thus fail to uncover the universal rules on effect of jamming on radar. Although the data-driven methods, e.g., convolutional neural networks [23], [24] and principle competent analysis [25], are utilized to address this issue by exploring the information hidden in the data (namely samples), this hurdle has not been completely tackled due to their black-box property.

In this work, we propose a novel evaluation method via associating signal-level evaluation and system/application-level evaluation together, aiming at simultaneously (i) keeping and combining the superiorities of the aforementioned two evaluation approaches and (ii) overcoming their respective drawbacks. To do so, we put forward a composite evaluation method based on RTFA and PAPR, where RTFA is exploited to directly analyze the TF spectrum of radar echoes for calculating the two-dimensional (2D) image entropy [26], [27] and PAPR determines a system/application-level evaluation by associating the SJR in radar processing chain and the performance of target detection. When they are combined together via normalization and weighted averaging, the composite parameters (i.e., normalization factors and weighting coefficients) are estimated from the samples, equipping the composite with data-adaptive property. Hence, we can derive a unified framework of evaluating the effect of jamming on radar and thus achieve the first aim (i). To refine the composite evaluation and accomplish the second objective (ii), we modify the traditional RTFA for signal-level evaluation and give theoretical guarantee of PAPR for system/application-level evaluation. On the one hand, different from the conventional RTFA [28]–[30], the modified RTFA can enhance the TF concentration, avoid the artifacts arising from the crossing terms and even cope with incomplete data in light of joint sparse model with convolution framelets, ultimately improving the precision of signal-level evaluation. On the other hand, target detection, usually viewed as a type of common and fundamental application that always affects the subsequent ones in radar, is used for the system/application-level evaluation to highlight the pertinence, and then we establish the quantitative relationship between SJR and detection probability by PAPR. Despite the well-defined PAPR [31], to the best of our knowledge, it is the first attempt to give theoretical guarantee of PAPR for evaluation. In the end, numerical experiments are designed to validate the feasibility and superiority of the proposed approach.

In summary, our contributions are as follows:

1) In term of signal-level evaluation, RTFA is exploited to estimate TF spectrum for calculating two-dimensional image entropy, where joint sparse model with convolution framelets is leveraged to improve TF concentration.
2) For system/application-level evaluation, we derive the variation of SJR in radar processing chain, and thus define the PAPR to associate SJR with target CFAR detection, leading to theoretical guarantee of PAPR for evaluation.
3) Composite evaluation based on RTFA and PAPR is proposed by computing the normalization factors and weighting coefficients from the training data and its feasibility and superiority is validated in numerical experiments.

The remainder of the paper is organized as follows. In Section II, we briefly overview the signal models for blanket jamming and PD radar. And then, Section III presents the evaluation approach in the sense of signal, i.e., signal-level evaluation, where the modified RTFA is proposed to analyze TF spectrum for calculating the 2D image entropy. In Section IV, we establish the quantitative relationship between SJR and detection probability by PAPR for system/application-level evaluation. The composite evaluation as well as the estimation of composite parameters are formulated in Section V. Section VI provides the numerical experiments to illustrate the feasibility and superiority of the proposed method. The conclusions are drawn in Section VII.

The notations and definitions employed in the paper are summarized in Table 1, where the lower-case letters denote scalars, boldface column lower-case letters denote vectors, and boldface upper-case letters denote matrices.

TABLE 1. Summary of frequently used symbols in this paper.

c	: the speed of light	j	: unit imaginary number
t	: time	f_0	: radar carrier frequency
$J(t)$	: jamming signal	$s(t)$	: radar signal
$\mathbf{x}$	: discrete signal	$\mathbf{S}$	: TF spectrum
$\mathbf{x}_m$	: signal patch of $\mathbf{x}$	$\mathbf{s}_m$	: frequency spectrum of $\mathbf{x}_m$
$\mathbf{X}$	: lifted signal of $\mathbf{x}$	$\mathbf{F}$	: Fourier basis
$\mathbf{\Phi}$	: $\mathbf{F}^{-1}$	$\mathbf{E}$	: unit matrix
$\mathbf{s}$	: vectorization of $\mathbf{S}$	$\mathbf{\Sigma}$	: convolution framelets
H	: 2D image entropy	P_s	: average power of true signal on x_0
SJR_0	: SJR of x_0	P_J	: average power of jamming on x_0
SJR_1	: SJR of x_1	P_s^1	: power of true signal at r_0 on x_1
SJR_2	: SJR of x_2	P_J^1	: power of jamming at r_0 on x_1
μ	: PAPR	P_s^2	: average power of true signal on x_2
w_H	: weighting for H	P_J^2	: average power of jamming on x_2
w_μ	: weighting for μ	P_t	: peak power of the target on x_2
F	: composite index	P_{fa}	: false alarm probability
		P_r	: detection probability

II. SIGNAL MODELS

In this section, we aim to briefly overview the signal models for blanket jamming and PD radar, providing the basis for evaluating the effect of blanket jamming. Unless otherwise specified, the symbols j, c, f_0, and t denote the unit imaginary number, the speed of light, carrier frequency, and time, respectively. For the sake of conciseness, we directly list the signal models for blanket jamming, i.e., RF noise, AM noise, FM noise and PM noise, as follows. RF noise, usually generated by filtering the white Gaussian noise (WGN), has the signal model of the form

$$J_{\text{RF}}(t) = U(t)\exp[j(2\pi f_0 t + \phi)], \tag{1}$$

where the amplitude $U(t)$ and the phase ϕ are independent random variables, satisfying Rayleigh distribution over $[0, +\infty)$ and uniform distribution over $(-\pi, \pi)$, respectively. However, according to this model, it is impractical to generate RF jamming with high power and wide bandwidth. For this reason, it is more popular to exploit other types of blanket jamming by modulating the related parameters by noise with different distributions. One of them is the AM jamming, i.e.,

$$J_{\text{AM}}(t) = [U + U(t)]\exp[j(2\pi f_0 t + \phi)], \tag{2}$$

where $U(t)$ satisfies generalized stationary random process over $[-U, +\infty)$ while ϕ, also independent with $U(t)$, satisfies an uniform distribution over $(0, 2\pi)$. Besides, FM jamming is usually modulated in a similar manner, and thus modeled as

$$J_{\text{FM}}(t) = U\exp[j(2\pi f_0 t + 2\pi K_1 \int_0^t u(s)ds + \phi)], \tag{3}$$

where the amplitude U and the frequency modulation ratio K_1 are constant numbers. Denotations $u(t)$ and ϕ are independent with each other and satisfy generalized stationary random process and uniform distribution over $(0, 2\pi)$, respectively. The last type of blanket jamming is the PM noise with the signal model

$$J_{\text{PM}}(t) = U\exp[j(2\pi f_0 t + K_2 u(t) + \phi)], \tag{4}$$

where the amplitude U and the phase modulation coefficient K_2 are also constant numbers. For $u(t)$ and ϕ, they follow the same meaning to that for FM jamming.

It is worth noting that any of the blanket jamming above has similar statistical character to WGN, when they are performed on radar systems. This mainly stems from the band-limited property of radar and will be discussed in section 4.1 for more details. Even so, different modulation modes of the four types of blanket jamming rely on different hardware systems, leading to different jamming parameters, e.g. intensity and bandwidth, for diverse application scenarios. Both of their similarity and difference provide convenience for effect evaluation by removing the redundancy and focusing on the critical details in blanket jamming.

When the echoes with blanket jamming come into radar systems, they are first processed by several steps before specific applications. It is well-known that these processing steps and the related applications are determined by the radar systems themselves, and so, at this point, we take into account the PD radar endowed with linear frequency modulation (LFM) signal for target detection as well as the subsequent applications (e.g. tracking). Despite various PD radar systems, the success of the considered PD radar above results from its good trade-off between ranging and velocity measurement. Furthermore, the processing chain in this radar system includes IFDC, matched filtering, MTI, CFAR detection and so on, and then we directly present the signal models of the major steps as follows.

For this PD radar, we start from the LFM signal

$$s(t) = \text{rect}(t/T)\exp[j2\pi(f_0 t + kt^2/2)], \tag{5}$$

where $\text{rect}(\cdot)$ is the rectangle envelope function and the symbols T, f_0, and k denote the time duration, the carrier frequency and the frequency modulation ratio, respectively. When the target with radial range $R(t)$ is assumed to have unit radar cross section (RCS), its echo can be given by

$$s_e(t) = s(t - t_0), \tag{6}$$

where $t_0 = 2R(t)/c$ is the time-delaying amount. With IFDC on $s_e(t)$, the signal is then formulated as

$$s_r(t) = \mathrm{rect}\left(\frac{t-t_0}{T}\right)\exp\left[j2\pi\left(-f_0t_0 + \frac{k(t-t_0)^2}{2}\right)\right], \tag{7}$$

Given the matched filter with response function $h(t) = s^*(t_1 - t)$, where $*$ is the conjugate operator and t_1 is the reference time, the filtered signal of $s_r(t)$ can be expressed as

$$x(t) = s_r(t) \circledast h(t), \tag{8}$$

where $\circledast$ is the convolution operator. Accordingly, the range of the target can be estimated from the signal $x(t)$, and also its radial velocity can be measured by the MTD on $x(t)$, i.e., filtering $x(t)$ with narrow-band filter banks.

When the radar works in jamming and noise environment, the echo in (6) becomes

$$\tilde{s}_e(t) = s_e(t) + J(t) + n(t), \tag{9}$$

where $J(t)$ is the blanket jamming signal and $n(t)$ is the noise arising from the other sources such as radar itself and ground/sea clutter. Despite the similar processing of $\tilde{s}_e(t)$ to $s_e(t)$ in PD radar, the performance of radar in jamming environment is usually degraded, suggesting the necessity of evaluating the effect of blanket jamming on radar. What's more, when $n(t)$ is comparable to $J(t)$ in intensity, the former can not be ignored (illustrated in Fig. 6). In practice, the intensity of $J(t)$, however, is usually much higher that of $n(t)$, especially when the jamming is deliberately designed. To be honest, even if it is difficult to ignore $n(t)$ in $\tilde{s}_e(t)$, we can also combine $J(t)$ and $n(t)$ together as both of them have similar statistics to WGN. For these reasons, we simplify (9) as

$$\tilde{s}_e(t) = s_e(t) + J(t), \tag{10}$$

where $n(t)$ has been omitted for conciseness.

The signal models of blanket jamming and the related processing steps in PD radar provide a forward model for evaluating the effect of jamming on radar. With this knowledge, in the following sections we will first research on the evaluations based on RTFA and PAPR, respectively, and then combine them by taking a weighted average with normalization factors and weighting coefficients estimated from samples.

III. EVALUATION BASED ON RTFA

Radar echoes with jamming directly carries the jamming information, allowing us to analyze the effect of jamming on radar in the sense of signal. It is also well-known that the TF spectrum of signal is of utmost importance in processing of echoes and recognition of jamming [16], [17], [19], [20], since the desirable TF spectrum of echoes strongly supports the good behavior of radar and the jamming also degrades the radar by destroying its normal TF spectrum. Starting from this point, we aim to implement the evaluation with the center of TF spectrum in this section. We first introduce the conventional RTFA methods and focus on their drawbacks, despite their superiorities. To address the limitations of conventional RTFA, we propose the modified RTFA approach by joint sparse model with convolution framelets. Based on the TF spectrum estimated by the proposed RTFA, a signal-level evaluation index, namely the 2D image entropy, is exploited to assess the effect of jamming on radar accurately. For clarity, we denote the (column) vector and the matrix by bold lowercase and uppercase letters, respectively, and also the symbols $\mathbb{R}$ and $\mathbb{C}$ indicate the real space and complex space, respectively.

A. CONVENTIONAL RTFA

To derive RTFA, we start from the conventional TF analysis for TF spectrum. Despite diverse TF analysis methods, they can be mainly categorized into three types, i.e., linear TF analysis, bilinear TF analysis and data-driven TF analysis (e.g. empirical mode decomposition). Linear TF analysis usually has low TF concentration while bilinear TF analysis can not remove the coupling effect that results from the crossing terms. For the data-driven type, even if it has high degree of flexibility on TF models, it lacks theoretical guarantee and so has much room for improvement of the robustness. Besides, it is difficult for conventional TF analysis to have good performance in extreme conditions, such as strong jamming and data missing. In this case, RTFA [28]–[30] provides a novel idea in framework of compressive sensing (or termed compressed sensing) to improve the robustness and accuracy of TF analysis.

To avoid the crossing terms of TF analysis for signals with multiple components, we start from one of the linear TF analysis methods, namely short time Fourier transform (STFT). Given the signal $x(t)$, its discrete formula, determined by sampling, can be written as $\mathbf{x} = [x_1, x_2, \cdots, x_M]^T$, where the superscript T is the transpose of matrices or vectors. According to STFT, the TF spectrum $\mathbf{S} = [\mathbf{s}_1, \mathbf{s}_2, \cdots, \mathbf{s}_M]$ of $\mathbf{x}$ can be expressed by

$$\mathbf{S}_{m,n} = \sum_{k=0}^{N-1} x_{m+k} \cdot \exp(-j2\pi kn/N), \tag{11}$$

where $m = 1, 2, \cdots, M$ and $n = 1, 2, \cdots, N$ are the discrete time and frequency, respectively, and the length-N rectangular window is utilized. For the sake of brevity, equation (11) can be reformulated into matrix form

$$\mathbf{s}_m = \mathbf{F} \cdot \mathbf{x}_m, \quad m = 1, 2, \cdots, M, \tag{12}$$

where $\mathbf{x}_m = [x_m, x_{m+1}, \cdots, x_{m+N-1}]^T$ is the mth signal patch extracted from original signal x. Clearly, some of the signal patches have the entries located outside of $\mathbf{x}$, and thus we can rearrange the original signal end to end to address this problem. It is worth noting that $\mathbf{F} \in \mathbb{C}^{N\times N}$ is the full-rank Fourier basis and has the inverse matrix $\mathbf{F}^{-1}$, so (12) can be rewritten as

$$\mathbf{x}_m = \mathbf{F}^{-1} \cdot \mathbf{s}_m, \quad m = 1, 2, \cdots, M. \tag{13}$$

Namely, the signal patch $\mathbf{x}_m$ can be linearly represented on the basis $\mathbf{F}^{-1}$ and the representation coefficient vector is $\mathbf{s}_m$.

Despite the linearity of STFT, it has much room for improvement of TF concentration and robustness. For this reason, RTFA is put forward to overcome these drawbacks by introducing the following optimization model

$$\min_{\mathbf{s}_m} \|\mathbf{s}_m\|_1 \ \text{ s.t. } \ \|\mathbf{x}_m - \mathbf{F}^{-1} \cdot \mathbf{s}_m\|_2^2 < \epsilon, \tag{14}$$

where $m = 1, 2, \cdots, M$, $\|\cdot\|_1$ is the ℓ_1 norm, and $\epsilon > 0$ is the parameter of error bounding. In fact, these optimization models can be numerically solved, respectively, and each solution is actually an estimation of the corresponding column of the TF spectrum $\mathbf{S}$. Notice that, in contrast to STFT in (11), RTFA can not only inherit its merit of avoiding the crossing terms, but also improve the TF concentration and the robustness by imposing the sparse constraint on spectrum estimation. Despite these superiorities, RTFA by (14) still has two major drawbacks: the sparse prior of original signal is explored locally, i.e., enforcing sparse constraint on each signal patch, and the computation complexity is high due to numerous optimization models.

An alternative method for RTFA can address the issues above by utilizing the joint sparse prior and the core is joint representation of $\mathbf{x}$ by its signal patches $\{\mathbf{x}_m\}_{m=1}^{M}$, i.e.,

$$\mathbf{x} = \begin{bmatrix} \mathbf{x}_1 \\ \mathbf{x}_{N+1} \\ \vdots \\ \mathbf{x}_{KN+1} \end{bmatrix} = \begin{bmatrix} \mathbf{F}^{-1} & \mathbf{0} & \cdots & \mathbf{0} \\ \mathbf{0} & \mathbf{F}^{-1} & \cdots & \mathbf{0} \\ \vdots & \vdots & \ddots & \vdots \\ \mathbf{0} & \mathbf{0} & \cdots & \mathbf{F}^{-1} \end{bmatrix} \begin{bmatrix} \mathbf{s}_1 \\ \mathbf{s}_{N+1} \\ \vdots \\ \mathbf{s}_{KN+1} \end{bmatrix}, \tag{15}$$

where $K = [M/N]$ is the maximum integer that is no more than M/N. With this linear representation of $\mathbf{x}$, a joint sparse model can be built and solved in a similar manner to (14), allowing us to explore the joint sparse prior of $\mathbf{x}$ and to reduce the computation cost by executing sparse recovery algorithm only once. Nevertheless, the signal patches used in (15) do not overlap with each other, and thus only some entries of $\{\mathbf{s}_m\}_{m=1}^{M}$, namely some columns in $\mathbf{S}$, are achieved, resulting in low time resolution of TF spectrum. It is also worth noting that the first equality in (14) do not hold strictly, because the right may be longer than the left. Although it has little or no effect on the aforementioned model and algorithm, the linear representation of $\mathbf{x}$ still has a minor defect, i.e., the representation basis (or dictionary) may not match original signal. In fact, the key point of tackling the two hurdles in joint sparse model lies in the exact sparse representation dictionary for $\mathbf{x}$, on which the sparse representation coefficients of $\mathbf{x}$ can be estimated for $\mathbf{S}$. Following this argument, we propose the modified RTFA using convolution framelets in next subsection.

B. MODIFIED RTFA

To tackle the issues in conventional RTFA, we put forward the modified RTFA in framework of convolution framelets. Notice that the models in (13) can be rearranged column by column as a matrix format

$$\mathbf{X} = \mathbf{\Phi} \cdot \mathbf{S}, \tag{16}$$

where $\mathbf{X} = [\mathbf{x}_1, \mathbf{x}_2, \cdots, \mathbf{x}_M]$, $S = [\mathbf{s}_1, \mathbf{s}_2, \cdots, \mathbf{s}_M]$ and $\mathbf{\Phi} = \mathbf{F}^{-1}$, and so the corresponding optimization model with joint sparse prior can be expressed as

$$\min_{\mathbf{S}} \|\mathbf{S}\|_1 \ \text{ s.t. } \|\mathbf{X} - \mathbf{\Phi} \cdot \mathbf{S}\|_2^2 < \epsilon. \tag{17}$$

Formally, this method for RTFA has achieved the joint sparse model with exact representation of $\mathbf{X}$ by $\mathbf{\Phi}$ and $\mathbf{S}$, however, despite the dependence of $\mathbf{X}$ on $\mathbf{x}$, original signal $\mathbf{x}$ is not equivalent to $\mathbf{X}$, suggesting the joint sparse constraint of $\mathbf{S}$ for $\mathbf{X}$ is invalid for $\mathbf{x}$. Indeed, the optimization model in (16) can be decomposed into the models in (14) equivalently, so it fails to solve the aforementioned problems in the essence.

Despite the hurdles of (15) and (16), they provide an exact representation model and a special structure of $\mathbf{X}$, namely the Hankel matrix. When the relationship between $\mathbf{x}$ and $\mathbf{X}$ can be achieved by this structure, we can also have that between $\mathbf{x}$ and $\mathbf{S}$ as well as the exact sparse representation dictionary, based on which the joint sparse model can be obtained accordingly. For the Hankel matrix, we have the following lemma:

Lemma 1: Assume $\mathbf{x} = [x_1, x_2, \cdots, x_M]^T \in \mathbb{R}^M$ and its corresponding Hankel matrix is defined by

$$\mathbf{X} = \begin{bmatrix} x_1 & x_2 & \cdots & x_M \\ x_2 & x_3 & \cdots & x_1 \\ \vdots & \vdots & \ddots & \vdots \\ x_N & x_{N+1} & \cdots & x_{N-1} \end{bmatrix} \in \mathbb{R}^{N\times M},$$

where N is the length of signal patches for x and $N < M$. And also, let $\circledast$ be circular convolution operator and $(\cdot)^{-}$ be the flip operator, namely $(\mathbf{v}^{-})_n = \mathbf{v}_{-n}$ for any vector $\mathbf{v}$. Then, we have

1) $\mathbf{x}_m = \frac{1}{N}\sum_{i=1}^{N} \mathbf{X}_{m-i+1,i}$, for $m = 1, 2, \cdots, M$;
2) $\mathbf{X} \cdot \mathbf{v} = \mathbf{x} \circledast \mathbf{v}^{-}$, for any $\mathbf{v} \in \mathbb{R}^N$;
3) $\mathbf{a}^T(\mathbf{b} \circledast \mathbf{c}) = \mathbf{b}^T(\mathbf{a} \circledast \mathbf{c}^{-})$, for any $\mathbf{a}, \mathbf{b} \in \mathbb{R}^M$ and $\mathbf{c} \in \mathbb{R}^N$.

The proof is simple and we omit it. It can be seen from Lemma 1 that the quantitative relationship between $\mathbf{x}$ and $\mathbf{X}$, as well as their property with respect to any given vector, has been shown exactly and the related equality for the operator $\circledast$ has been also formulated for further investigation of convolution framelets.

For the sake of clarity, we first present the representation lemma for $\mathbf{x}$ and $\mathbf{X}$:

Lemma 2: Assume that $\mathbf{U} \in \mathbb{R}^{N\times N}$ and $\mathbf{V} \in \mathbb{R}^{M\times M}$ are orthogonal matrices, and let $\{\mathbf{u}_i\}_{i=1}^{N}$ and $\{\mathbf{v}_j\}_{j=1}^{M}$ be their column vectors, respectively. For any vector $\mathbf{x} \in \mathbb{R}^M$ and its Hankel matrix $\mathbf{X} \in \mathbb{R}^{N\times M}$, where $N < M$, we have

1) $\mathbf{X} = \mathbf{U}\mathbf{\Gamma}\mathbf{V}^T$, where $\mathbf{\Gamma}_{ij} = \mathbf{x}^T(\mathbf{u}_i \circledast \mathbf{v}_j)$;
2) $\mathbf{x} = \frac{1}{N}\sum_{i=1}^{N}\sum_{j=1}^{M} \mathbf{\Gamma}_{ij}\mathbf{u}_i \circledast \mathbf{v}_j$.

The proof is also presented in Appendices. It is well-known that singular value decomposition (SVD) has been widely applied in matrix analysis for signal processing, and so it is amazing that the Hankel matrix $\mathbf{X}$ in Lemma 2 has a SVD-like decomposition. This decomposition, however, is more general as $\mathbf{U}$ and $\mathbf{V}$ are arbitrary orthogonal matrices. Accordingly, $\mathbf{x}$ also has a new representation formula on the vector set $\{\mathbf{u}_i \circledast \mathbf{v}_j | i = 1, 2, \cdots, N, j = 1, 2, \cdots, M\}$, which actually corresponds to a tight frame termed convolution framelets. The following lemma provides a theoretical guarantee:

Lemma 3 ([32]): Assume that $\mathbf{U} \in \mathbb{R}^{N\times N}$ and $\mathbf{V} \in \mathbb{R}^{M\times M}$ are the orthogonal matrices, respectively, and denote by $\{\mathbf{u}_i\}_{i=1}^N$ and $\{\mathbf{v}_j\}_{j=1}^M$ their column vectors, respectively. If $N < M$, the vectors $\mathbf{u}_i \circledast \mathbf{v}_j$ for $i = 1, 2, \cdots, N$ and $j = 1, 2, \cdots, M$ form a tight frame for $\mathbb{R}^M$ with frame constant N.

With lemma 2 and lemma 3, let's now go back to the representation problem of $\mathbf{X}$ in (16). To explore the joint sparse prior and reduce the computation cost for RTFA, we have a new linear representation of $\mathbf{x}$ using convolution framelets.

Theorem 1: Assume that $\mathbf{x} \in \mathbb{C}^M$ and its Hankel matrix is $\mathbf{X} \in \mathbb{C}^{N\times M}$. Also let $\mathbf{\Phi} \in \mathbb{C}^{N\times N}$ and $\mathbf{E} \in \mathbb{R}^{M\times M}$ be the inverse Fourier basis and the unit matrix, respectively. If $\mathbf{X} = \mathbf{\Phi} \cdot \mathbf{S}$ holds for $\mathbf{S} \in \mathbb{C}^{N\times M}$, then we have the linear representation $\mathbf{x} = \mathbf{\Sigma s}$, where $\mathbf{s}$ is the vectorization of $\mathbf{S}$ and $\mathbf{\Sigma}$ is the convolution framelets constructed from $\mathbf{\Phi}$ and $\mathbf{E}$.

The proof is shown in Appendices. It is worth noting that the signal $\mathbf{x}$, as well as $\mathbf{X}$, in the lemmas above is assumed to be located in the real space, while it has been extended into the complex space in Theorem 1, since almost all of the signals used in effect evaluation of blanket jamming on radar are complex. Moreover, as shown in Theorem 1, convolution framelets offers an exact representation of $\mathbf{x}$, i.e., $\mathbf{x} = \mathbf{\Sigma s}$, which leads to a quantitative and direct relationship between $\mathbf{x}$ and its TF spectrum $\mathbf{S}$ and so avoids the loss of time/frequency resolution. More importantly, the sparseness of $\mathbf{x}$ can be enhanced by the over-completeness of convolution framelets, improving the performance of the sparsity-based models and algorithms.

Based on convolution framelets, the proposed optimization model for RTFA can rewritten as

$$\min_{\mathbf{s}} \|\mathbf{s}\|_1 \;\; \text{s.t.} \; \|\mathbf{x} - \mathbf{\Sigma s}\|_2^2 < \epsilon. \tag{18}$$

This model can be numerically solved by sparse recovery algorithms, such as OMP, BP, SP, and so on [33], [34]. Once the solution $\hat{\mathbf{s}}$ is achieved, then the TF spectrum $\mathbf{S}$ can be estimated by reshaping $\hat{s}$ into a matrix of dimension $N \times M$. As we have argued, the proposed method for RTFA can not only avoid the artifacts from the crossing terms by using linear representation instead of the bilinear one, but also improve the TF concentration as well as the robustness to noise and data-missing by enforcing joint sparse constraint via convolution framelets. Meanwhile, in contrast to conventional RTFA, the computation complexity can also be reduced by the proposed RTFA as the model size has been decreased and the algorithm is executed only once.

Finally, we aim to a remark on the convolution framelets used for the proposed RTFA. Although the modified RTFA starts from STFT, namely the Fourier basis is used to construct convolution framelets, many popular bases, e.g., Gabor basis, wavelet basis, etc., can be also unitized for the modified RTFA. Specifically, if the matrix $\mathbf{\Phi}$ in Theorem 1 is regarded as the representation basis for $\mathbf{x}$ in the dimension of frequency, the matrix $\mathbf{E}$ is actually the representation basis in the dimension of time, which can be also replaced by other bases. In this case, we can make use of the modified RTFA to achieve the generalized TF spectrum, providing high degree of freedom in effect evaluation of blanket jamming on radar.

C. EVALUATION INDEX: 2D IMAGE ENTROPY

Now let us go back to our original task, i.e., evaluating the effect of blanket jamming on radar. Since the modified RTFA provides the accurate TF spectrum of the echoes with jamming, a quantitative index is definitely needed to assess its quality for effect evaluation. It is well-known that the echoes with different jamming types or parameters always have different TF spectrums, namely that with different intensities or distributions. When the TF spectrums are regarded as images, we can directly exploit the image entropy to measure the difference on TF spectrums. In fact, entropy is first proposed in information theory and its success results from the fact that entropy means the richness of information.

There are two types of image entropy and the first is one-dimensional (1D) image entropy with the definition $\sum_{i=0}^{L} p_i \log p_i$, where L is the image gray level and p_i is ratio of the pixels with gray i to the total. The 1D image entropy can measure the concentration of image energy, while it fails to reflect the energy distribution. For this reason, we take into account the second image entropy, i.e., the 2D image entropy [26], [27]. Formally, it is defined as

$$H = -\sum_{i=0}^{L}\sum_{j=0}^{L} p_{ij} \log p_{ij} \tag{19}$$

with

$$p_{ij} = \frac{f(i,j)}{N}. \tag{20}$$

Here N is the number of pixels on the image and $f(i,j)$ is the number of the pixel pair (i,j), where i denotes the current pixel value and j is the mean value of the adjacent pixels of the current pixel. The 2D image entropy is more robust than the 1D image entropy and its feasibility for effect evaluation will be illustrated in the following experiments.

IV. EVALUATION BASED ON PAPR

The signal-level evaluation based on RTFA has been implemented in the section above, and now we put emphasis on the system/application-level evaluation based on PAPR. As we have argued in introduction, we aim to deal with two issues in system-level evacuation, namely (a) various applications of PD radar result in the lack of unified evaluation framework and the difficulty of transferring the evaluation from one application to the others, and (b) the traditional methods for system/application-level evaluation always depend on the simulations and experiments and so fail to uncover the jamming mechanism and to provide theoretical guarantee. To address the issue (a), we view CFAR detection as the kernel application for PD radar, since it is a type of common and fundamental application that usually affects the subsequent ones. In other words, if CFAR detection does not have good performance, the subsequent applications also can not work well. In the sequel, CFAR detection can provide a unified evaluation standard for the system/application-level evaluation. Whereas, if the detection probability for CFAR detection is directly exploited as the evaluation index to solve issue (a), issue (b) still remains. For this reason, we establish the quantitative relationship between SJR and detection probability by the PAPR, thus giving theoretical guarantee of the PAPR for system/application-level evaluation.

As a result, the first step towards realizing the idea above is to analyze the statistics of blanket jamming in PD radar, based on which the variation of SJR in processing chain of PD radar can be measured quantitatively and then the evaluation index RAPR is proposed. Also, the theoretical guarantee of the PAPR is given for CFAR detection, suggesting that the PAPR can tackle the issues (a) and (b) simultaneously.

A. APPROXIMATE STATISTICS OF BLANKET JAMMING

To tackle the issues above, the statistics of blanket jamming are first analyzed for the evaluation index PARP in this subsection. Although the signal models of blanket jamming and PD radar have been introduced in section 2, the statistics of blanket jamming have not been explored enough, especially when the jamming signals are processed in the processing chain of PD radar. In practice, their statistics would be always changed due to the band-limited property of PD radar, allowing us to derive a unified approximate statistical distribution for different blanket jamming types.

For conciseness, when the blanket jamming signals are processed by IFDC step in PD radar, their models can be directly expressed as

$$\begin{cases} \bar{J}_{\mathrm{RF}}(t) = U(t)\exp(j\phi) \\ \bar{J}_{\mathrm{AM}}(t) = [U + U(t)]\exp(j\phi) \\ \bar{J}_{\mathrm{FM}}(t) = U\exp[j(2\pi K_1 \int_0^t u(s)ds + \phi)] \\ \bar{J}_{\mathrm{PM}}(t) = U\exp[j(K_2 u(t) + \phi)], \end{cases} \tag{21}$$

respectively, where the carrier frequency f_0 has been cancelled by IFDC. First of all, we take into account the RF jamming. As we have argued, its amplitude $U(t)$ and phase ϕ are independent random variables and satisfy Rayleigh distribution and uniform distribution, respectively, so it can be decomposed into two orthogonal random variables. If it is rewritten as $\bar{J}_{\mathrm{RF}}(t) = U^a(t) + jU^b(t)$, then we have

$$\begin{cases} U^a(t) = U(t)\cos(\phi) \\ U^b(t) = U(t)\sin(\phi), \end{cases} \tag{22}$$

where both of $U^a(t)$ and $U^b(t)$ satisfy Gaussian distribution, namely normal distribution. In this case, when the RF jamming is processed by IFDC, we can conclude that it can be modeled as the random variable satisfying the complex Gaussian distribution.

After analyzing the RF jamming, we now focus on the AM jamming, where we have the similar results. It is worth noting that, when some conditions are satisfied, AM jamming can degenerates to RF jamming. For instance, if its amplitude is rewritten as

$$\bar{U}(t) = U + U(t) = \sqrt{\frac{\pi}{2}} \cdot \sigma + U(t), \tag{23}$$

where σ^2 is the variance of $U(t)$, then it would appear that $\bar{U}(t)$ approximately or exactly satisfies the Rayleigh distribution over $[0, +\infty)$, depending the choice of the generalized stationary random process over $[U, +\infty)$ for $U(t)$. In other words, AM jamming can be also statistically modeled by the complex Gaussian distribution approximately.

With repeat to FM jamming and PM jamming, their modulation noise $u(t)$ in (21) is usually assumed as Gaussian random variable, and thus their power spectrum densities also approximately satisfy the Gaussian distribution. More importantly, notice that both of them have wide bandwidth, within which their instant frequency varies continuously and dramatically; while the receiver in PD radar has both of relatively narrow system bandwidth and time-delaying sluggishness. For this reason, the jamming waveforms that come into the receiver can be viewed as continuous random shock composed of overlapping bell-like pulses instead of the separate sharp ones. After IFDC step, the envelope and the phase of FM jamming and PM jamming also approximately satisfy Rayleigh distribution and uniform distribution, respectively, providing the similar statistics to RF jamming.

In conclusion, the four types of blanket jamming can approximately or exactly satisfy the complex Gaussian distribution, when they come into PD radar and are processed by IFDC step. Their unified approximate statistical distribution stems from both of their original statistics and the bandwidth-limited property of PD radar and is also supported by the central limit theorem in theory. The feasibility of this approximation can be also illustrated in the following experiments, by the similar effect curves of different types of blanket jamming under the same simulated conditions.

B. EVALUATION INDEX: PAPR

Depending on the signal models in section 2 and the approximate statistics of blanket jamming, the variation of SJR in processing chain of PD radar is first derived explicitly and then the index PAPR is proposed for system/application-level evaluation. It is worth noting that SJR is an fundamental but important conception that will be used frequently in the following. Unless specifically declared, SJR corresponds to the ratio of average power; however, it refers to that of instantaneous power when the SJR at some time or in some space is used. If the power is uniformly distributed over the whole domain, i.e., the average power equals to the instantaneous power, there is no difference between them; otherwise, it is more likely that they are nonequivalent to each other.

Following the assumptions and denotations in section 2, we assume that N_r and N_a are the number of samples for each LFM signal and that of echoes, respectively, which are actually the sampling numbers on the dimensions of range and azimuth, respectively. In particular, when the sampling frequency and the pulse repetition frequency (PRF) are given, they are determined by their corresponding durations directly. Also, we denote by $J_0(t)$ and $s_0(t)$ the blanket jamming signal and the true signal from a target after IFDC step, respectively, and thus the signal for matched filtering can be given by

$$\begin{aligned} x_0(t_m, \hat{t}) &= s_0(t_m + \hat{t}) + J_0(t_m + \hat{t}) \\ &\triangleq s_0(t_m, \hat{t}) + J_0(t_m, \hat{t}), \end{aligned} \tag{24}$$

where the slow time t_m and the fast time $\hat{t}$ satisfy $t = t_m + \hat{t}$. If the jamming signal and the true signal have the average power P_J and P_s, respectively, the SJR of x_0 can be measured by

$$\mathrm{SJR}_0 = 10\log_{10}(P_s/P_J). \tag{25}$$

According to matched filtering principle in (8), the signal in (24) is filtered by $h(\cdot)$ and we have

$$\begin{aligned} x_1(t_m, r) &= x_0(t_m, \hat{t}) \otimes h(\hat{t}) \\ &= s_0(t_m, \hat{t}) \otimes h(\hat{t}) + J_0(t_m, \hat{t}) \otimes h(\hat{t}) \\ &\triangleq s_1(t_m, r) + J_1(t_m, r), \end{aligned} \tag{26}$$

where $r = c\hat{t}/2$. It is well-known that $s_1(t_m, r)$ in (26) refers to the desirable (ideal) result of matched filtering and has the form

$$s_1(t_m, r) \approx C_1 \mathrm{sinc}[k_1(r - r_0)] \exp(-j2\pi f_d t_m), \tag{27}$$

where r_0 is the target's radial range and f_d is the Doppler frequency shift caused by the target's radical velocity. For conciseness, the high-order terms with respect to t_m are ignored and the constants in PD radar are combined into the constant numbers C_1 and k_1. In this case, we have the following lemma on the variation of SJR stemming from matched filtering, namely,

Lemma 4: Assume that x_1 in (26) is achieved by filtering x_0 in (24) via matched filtering. If J_0 in (24) satisfies complex Gaussian distribution, at r_0 we have

$$\mathrm{SJR}_1 = \mathrm{SJR}_0 + 10\log_{10}(k_r N_r),$$

where SJR_0 and SJR_1 are the SJR values of x_0 and x_1, respectively, and k_r is a radar system constant.

Now we briefly present the proof of the lemma above. According to the definition of SJR, its value of x_1 at r_0 can be computed by

$$\mathrm{SJR}_1 = 10\log_{10}(P_s^1/P_J^1),$$

where P_s^1 and P_J^1 are the power of the true signal and the jamming signal at r_0, respectively. Matched filtering principle tells that $P_s^1 = P_s \cdot k_r N_r$ is actually the energy of the LFM signal (in discrete version) with radar system constant k_r and that $P_J^1 = P_J$ holds for the jamming noise with complex Gaussian distribution. In the sequel, by taking these equations into SJR_1, the result in Lemma 4 is achieved and the proof is completed. What is more, we have to mention that the constant k_r actually depends on the PD radar itself, such as system gain and loss. The significance of Lemma 4 lies in the fact that it not only quantitatively describes the variation of SJR arising from matched filtering, but also provides the theoretical basis for analyzing the effect of MTD on SJR.

Next, we aim to analyze the variation of SJR arising from MTD. Starting from the signal $x_1(t_m, r)$ in (26), narrow-band filter banks are usually used to filter the signals for detecting the Doppler frequency shift caused by target's radical velocity. For the sake of clarity, we directly exploit the Fourier transform to implement the MTD, namely

$$\begin{aligned} x_2(f, r) &= \int_0^{T_a} x_1(t_m, r) e^{-j2\pi f t_m} dt_m \\ &= \int_0^{T_a} s_1(t_m, r) e^{-j2\pi f t_m} dt_m \\ &\quad + \int_0^{T_a} J_1(t_m, r) e^{-j2\pi f t_m} dt_m \\ &\triangleq s_2(f, r) + J_2(f, r), \end{aligned} \tag{28}$$

where T_a is the duration of echoes in azimuth dimension. Similarly, the variation of SJR arising from MTD is shown as follows:

Lemma 5: Assume that x_2 in (28) is achieved by transforming x_1 in (26) via MTD. If J_1 in (26) satisfies complex Gaussian distribution, at $(-f_d, r_0)$ we have

$$\mathrm{SJR}_2 = \mathrm{SJR}_1 + 10\log_{10}(k_a N_a),$$

where SJR_1 and SJR_2 are the SJR values of x_1 and x_2, respectively, and k_a is a radar system constant.

The proof is shown in Appendices. Lemma 5 also tells that the energy of $x_2(f, r)$ will be concentrated on $(-f_d, r_0)$, which are determined by the target's radical velocity and range, respectively. In this case, it is possible to detect the target from the signal $x_2(f, r)$, and thus the PAPR for $x_2(f, r)$ can be defined as

$$\mu = 10\log_{10}\left(\frac{P_t}{P_J^2}\right), \tag{29}$$

where P_t and P_J^2 are the peak power of the target and the average power of the jamming. At $(-f_d, r_0)$, we have $P_t = P_s^2 + P_J^2$, where P_s^2 and P_J^2 are the powers of the true signal and the jamming of $x_2(f, r)$, respectively. It is therefore easy to conclude

$$\mu = 10\log_{10}\left(\frac{P_s^2}{P_J^2} + 1\right) = 10\log_{10}\left(10^{\frac{\mathrm{SJR}_2}{10}} + 1\right). \tag{30}$$

Although the PAPR μ is proposed for target detection, it has close relation to SJR. In practice, by associating lemma 4, lemma 5 and equation (30) together, we have the following theorem:

Theorem 2: For PD radar with LFM signal and blanket jamming, assume that N_r and N_a are its sampling numbers on range and azimuth, respectively. If the SJR of x_0 in (24) is SJR_0 and the PAPR of x_2 in (28) is μ, we have

$$\mu = 10\log_{10}\left(k \cdot 10^{\frac{\mathrm{SJR}_0}{10}} + 1\right),$$

where $k = k_r N_r \cdot k_a N_a$ with radar system constants k_r and k_a. In particular, if the jamming power is so small that $k \cdot 10^{\frac{\mathrm{SJR}_0}{10}} \gg 1$, we have $\mu \approx \mathrm{SJR}_0 + 10\log_{10} k$; otherwise, if $k \cdot 10^{\frac{\mathrm{SJR}_0}{10}} \ll 1$, $\mu \approx 0$.

For conciseness, the proof of the theorem above is omitted. This theorem shows the quantitative relationship between the PAPR and the SJR, where the SJR is also directly determined by the blanket jamming as well as radar system; thus the PAPR depends on the blanket jamming once the radar system is given. Furthermore, the PAPR can also determine the performance of CFAR detection, which will be discussed in the following subsection. For this reason, the PAPR is used as a system/application-level index to evaluate the effect of blanket jamming on PD radar.

C. THEORETICAL GUARANTEE OF PAPR FOR CFAR DETECTION

It is well-known that CFAR detection is a foundational but important application for PD radar, which has remarkable influence on the subsequent applications. Therefore, the detection probability is usually used to assess the performance of radar in jamming environment by experiments or simulations. At this point, we aim to establish the quantitative relationship between the PAPR and the detection probability for CFAR detection to avoid the high computation cost and to provide theoretical guarantee for system/application-level evaluation.

In light of the approximate statistics of blanket jamming and the linearity of the processing chain in PD radar, the jamming $J_2(f, r)$ of $x_2(f, r)$ in (28) approximately satisfies the complex Gaussian distribution. Thus, the signal $y = |x_2|^2$ obtained by the square-law detector satisfies the exponential distribution [35], i.e.,

$$f(y; \eta) = \frac{1}{\eta}\exp\left(-\frac{y}{\eta}\right), \quad y \geq 0, \tag{31}$$

where $\eta > 0$ is the statistical parameter. When only the jamming exists, we have $\eta = P_J^2$, where P_J^2 is the power of jamming in x_2; otherwise, we have $\eta = P_t = P_s^2 + P_J^2$, where P_t and P_s^2 denote the peak power of x_2 and the power of the target (at $(-f_d, r_0)$) in x_2, respectively. According to CFAR detection, if the detection thresholding $T_d (> 0)$ is given, the false alarm probability P_{fa} can be estimated by

$$P_{fa} = \int_{T_d}^{+\infty} f(y; \eta = P_J^2)dy = \exp(-T_d/P_J^2), \tag{32}$$

leading to $T_d = -P_J^2 \cdot \ln P_{fa}$. Likewise, the detection probability P_r by CFAR detection can be written as

$$P_r = \int_{T_d}^{+\infty} f(y; \eta = P_s^2 + P_J^2)dy = (P_{fa})^{\left(\frac{P_s^2}{P_J^2}+1\right)^{-1}}. \tag{33}$$

Taking (30) and (32) into (33), we have the relationship between the PAPR and CFAR detection, which is summarized as follows.

Theorem 3: For PD radar and CFAR detection, the PAPR μ determines the logarithmic linear relation between detection probability P_r and false alarm probability P_{fa}, i.e.,

$$\ln(P_r) = 10^{-\mu/10} \cdot \ln(P_{fa}),$$

where $\ln(\cdot)$ is the natural logarithm operator.

Notice that Theorem 3 presents the quantitative relationship between PAPR and CFAR detection and Theorem 2 reveals that between SJR and PAPR, so the PAPR has built the bridge between the blanket jamming and the application of PD radar, which not only partly uncovers the jamming mechanism of blanket jamming on PD radar, but also provides the theoretical guarantee of PAPR for system/application-level evaluation.

V. COMPOSITE EVALUATION

Although the signal-level index (i.e., the 2D image entropy H based on RTFA) and the system/application-level index (i.e., the PAPR μ) have been constructed in section 3 and in section 4, respectively, it is still difficult to make a final decision when they are not completely consistent to each other. To solve this intractable issue, we composite them together using normalization and weighted averaging. The composite evaluation can combine their advantages and improve the evaluation robustness as well as the conveniences in practical applications.

The first step towards compositing the indices is normalization as they have different dimensions, and then their weighted average is computed. Therefore, the key point for composite evaluation lies in the design of normalization factors and weighting coefficients. Inspired by data mining, they can be estimated from the samples achieved under different jamming conditions (e.g., types and parameters), exploring the information hidden in samples sufficiently and improving the robustness. Without loss of generality, for given radar system, the samples are achieved with different jamming types and different SJR values. Concretely speaking, we set M different SJR values for each of the four blanket jamming types (namely RF, AM, FM and PM), and so there are $4M$ jamming property labels for samples. To enhance the robustness, N samples are achieved for each jamming property label, and thus we have $4MN$ samples in database, i.e., $\mathcal{J} = \{J_{mn}^k | m = 1, 2, \cdots, M; n = 1, 2, \cdots, N; k = 1, 2, 3, 4.\}$. In fact, besides the property labels, there are also the signals used to compute or estimate the indices H and μ for each entry in $\mathcal{J}$. For conciseness, we directly show the corresponding index values H_{mn}^k and μ_{mn}^k for $J_{mn}^k \in \mathcal{J}$. Since the robustness of the indices can be enhanced by averaging over N samples, we take a average of the index values for each jamming property label, i.e.,

$$\begin{cases} H_m^k = \frac{1}{N}\sum_{n=1}^{N} H_{mn}^k \\ \mu_m^k = \frac{1}{N}\sum_{n=1}^{N} \mu_{mn}^k, \end{cases} \tag{34}$$

where $m = 1, 2, \cdots, M$ and $k = 1, 2, 3, 4$.

On normalization, we exploit the extreme values in $\{H_m^k | m = 1, 2, \cdots, M; k = 1, 2, 3, 4\} \triangleq \mathcal{H}$ and $\{\mu_m^k | m = 1, 2, \cdots, M; k = 1, 2, 3, 4\} \triangleq \mathcal{Q}$ to normalize the two evaluation indices, respectively, canceling the difference of dimensions. The normalization factors are therefore obtained by

$$\begin{cases} H_{\max} = \max\ \mathcal{H} \\ H_{\min} = \min\ \mathcal{H}, \end{cases} \tag{35}$$

and

$$\begin{cases} \mu_{\max} = \max\ \mathcal{Q} \\ \mu_{\min} = \min\ \mathcal{Q}. \end{cases} \tag{36}$$

Thus the normalized indices for signal-level evaluation and the system/application-level evaluation can be expressed, respectively, by

$$\begin{cases} \hat{H} = g\left(\frac{H - H_{\min}}{H_{\max} - H_{\min}}\right) \\ \hat{\mu} = g\left(\frac{\mu_{\max} - \mu}{\mu_{\max} - \mu_{\min}}\right) \end{cases} \tag{37}$$

where $g(\cdot)$ is the truncation function defined as

$$g(t) = \begin{cases} 0, & t < 0 \\ t, & t \in [0, 1] \\ 1, & t > 1 \end{cases} \tag{38}$$

The introduction of $g(\cdot)$ can normalize its input into [0, 1] and help to deal with the issue that the index values of testing signals are out of the range defined by the extreme values. Besides, it is well-known that the normalization heavily depends on the samples, because they actually determine the extreme values. Although it is hard to include all of the possible jamming property labels in the sample set $\mathcal{J}$, this set should be still expanded as large as possible. For instance, some important cases of jamming property labels, e.g. the jamming-free signals, are also necessary to be added to the sample set in practice. It is also worth noting that the formulas of H and μ as the inputs of $g(\cdot)$ in (38) are inconsistent to each other, which stems from the fact that the indices H and μ have different variation trends as SJR decreases or increases.

On weighted averaging, we also start from the index sets $\mathcal{H}$ and $\mathcal{Q}$ of the sample set $\mathcal{J}$. Taking into account the difficulty of comparing the importance of H and μ in evaluation, we exploit the separability of $\mathcal{H}$ and $\mathcal{Q}$ to estimate their weighting coefficients. It is well-known that the separability of features plays a leading role in classification and recognition, since high separability of features usually helps to improve the efficiency of classification and recognition. Similarly, the evaluation efficiency from H and μ also relies on their separabilities, respectively. Therefore, the weighting coefficients are estimated by

$$\begin{cases} w_H = \sigma_H / \bar{H} \\ w_\mu = \sigma_\mu / \bar{\mu}, \end{cases} \tag{39}$$

where σ_H and $\bar{H}$ are the standard deviation and mean of $\mathcal{H}$, respectively, and σ_μ and $\bar{\mu}$ are that of $\mathcal{Q}$, respectively. These definitions above not only describe the separability sufficiently, but also avoid the hurdle from the dimension difference.

Associating the normalization factors and the weighting coefficients estimated from samples, the composite evaluation index F can be achieved by weighted averaging, namely,

$$F = \frac{w_H}{w_H + w_\mu}\hat{H} + \frac{w_\mu}{w_H + w_\mu}\hat{\mu}, \tag{40}$$

where $\hat{H}$ and $\hat{\mu}$ are defined in (37). Once the evaluation indices H and μ are computed for the given jamming, targets and PD radar, the composite evaluation index F can be estimated by (40). The definition of F also tells that $F = 0$ means there is no jamming or the jamming is so slight that it can be ignored; while $F = 1$ implies that the effect of the jamming on radar is similar to that of the heaviest jamming in sample set. Its feasibility and robustness in practical applications will be illustrated in the following numerical experiments.

In the end, we aim to give some remarks. Notice the composite evaluation depends on RTFA and PAPR, but in theory it is difficult to determine which is more significant in exploring the jamming mechanism. Since the RTFA-based evaluation and the PAPR-based evaluation actually perform in the viewpoints of signal and application, respectively, they can make their own contributions to effect evaluation of blanket jamming on radar. However, in application their performance can be measured by the weighting coefficients for composite evaluation, namely, the evaluation method (RTFA or PAPR) with larger weighting coefficient is more significant than the other one. In fact, in different cases of radar and jamming they can have different performance in effect evaluation. That is to say, in some cases the RTFA-based evaluation may have larger weighting coefficient than the PAPR-based evaluation, while in other cases the opposite result may be achieved. That is why we make use of the composite evaluation to combine the advantages of RTFA and PAPR, and thus the composite evaluation can be robustly applied to more complex cases of radar and jamming.

VI. NUMERICAL EXPERIMENTS

In this section, numerical experiments are performed to illustrate the behavior of the signal-level index, the system/application-level index, and their composite index for evaluating the effect of blanket jamming on PD radar. The superiority of the proposed RTFA is first validated by comparing with different TF analysis methods on the accuracy, the resolution and the artifacts arising from crossing terms, after which the signal-level evaluation index, namely 2D image entropy, is computed for different TF spectrums of the same signal to show the significance of the proposed method for evaluation. And then, by presenting the visual effects of matched filtering and MTD and computing the PAPR under different jamming conditions, we aim to illustrate the main results in Theorem 2 and to reveal the dominant role of PAPR in exploring the jamming mechanism. In the end, the feasibility and the robustness of composite evaluation is validated by analyzing its variation trends under different jamming types and parameters as well as by estimating the consistency in term of the correlation coefficients between composite index and detection probability of CFAR detection, which also supports Theorem 3 indirectly.

Unless specified otherwise, we will have the following setting for PD radar, target and jamming in numerical experiments. Assume that the PD radar transmits the LFM signal and its carrier frequency, bandwidth, pulse duration and PRF are set as 1GHz, 5MHz, 10μs and 10KHz, respectively. Moreover, the sampling frequency and the SNR of the receiver are set as 20MHz and 20dB, respectively. With respect to the target, its radical range, radial velocity and RCS are set as 10km, 100m/s and 1m^2, respectively. Meanwhile, we utilize the four types of blanket jamming with the signal models shown in section 2 to simulate the jamming, where $K_1 = 3 \times 10^7$ and $K_2 = \pi/2$ are set for FM jamming in (3) and PM jamming in (4), respectively. Also, we take a average of experimental results over 100 Monte Carlo simulations, improving the robustness of numerical experiments.

A. RTFA

In numerical experiments of TF analysis, we assume that four targets with the same parameters to the aforementioned target are located at 10km, 10.5km, 11km, and 12.3km, respectively, and that the blanket jamming has the SJR of -15dB. For the proposed RTFA, the model in (18), with length-63 signal patches and the parameter $\epsilon = 10^{-3}$, is numerically solved by basis pursuit algorithm with stopping thresholding 10^{-6}. As compared methods, smooth pseudo Wigner-Ville (SPWV) distribution and STFT are exploited, where the length-63 'Kaiser' time window or/and the length-15 'Kaiser' frequency window are used.

First of all, we show in Fig. 1 the echo of four targets in jamming-free environment and its distributions achieved by the aforementioned three methods. Clearly, four components of LFM signals can be observed from the TF distributions due to the jamming-free environment. Furthermore, despite the higher TF resolution from SPWV, STFT has no artifacts arising from the crossing terms. Also, STFT has higher accuracy than SPWV, as the bandwidth observed from Fig. 1c exactly equals to the given bandwidth 5MHz while that from Fig. 1b does not. In other words, the frequency in Fig. 1c varies from -2.5MHz to 2.5MHz while that in Fig. 1b varies from -4.5MHz to 4.5MHz, so the frequency bandwidth estimated from Fig. 1c has higher accuracy than that from Fig. 1b.

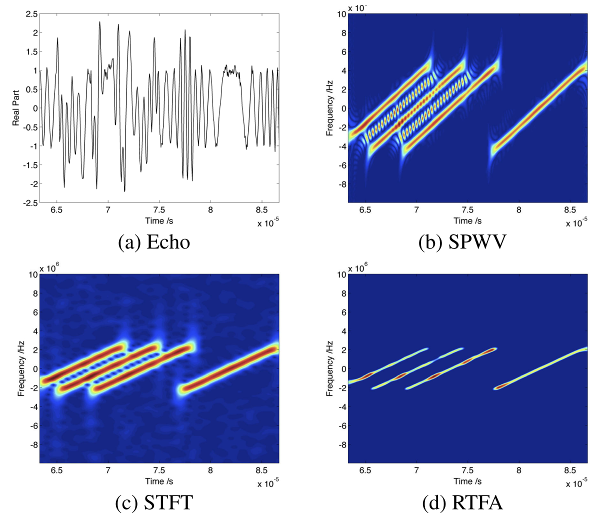

FIGURE 1. Echo of four targets in jamming-free environment and its TF distributions.

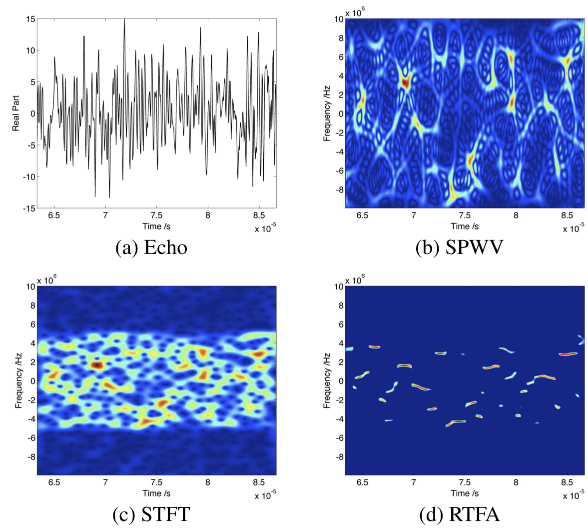

FIGURE 2. Echo of four targets in RF jamming environment and its TF distributions.

The proposed RTFA not only has the same accuracy to STFT and avoids the artifacts, but also achieves a higher TF resolution than SPWV, giving us an accurate estimation of TF spectrum for computing the 2D image entropy.

Likewise, we also present the results in jamming environment in Fig. 2, where RF jamming is only considered for conciseness. Because of strong RF jamming, the waveform (in real part) in Fig. 2a remarkably differs from that in Fig. 1a, but the superiority of the proposed RTFA is still retained. The TF distributions in Fig. 2c and Fig. 2d also imply the bandwidth-limited property of radar, i.e., the bandwidth of signals in the processing chain of radar is always limited within a finite range, despite the jamming with large bandwidth. Moreover, in contrast of that in Fig. 1, the TF spectrum of four targets in Fig. 2 disappears, the reason of which lies

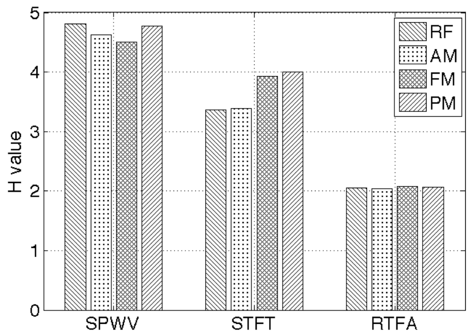

FIGURE 3. The H values for blanket jamming with the SJR of -15dB.

in the fact that the true signals are suppressed by the strong jamming successfully.

To validate the superiority of the proposed RTFA for signal-level evaluation, we also compare the robustness of the 2D image entropy to jamming types for the three TF analysis methods. These jamming types include RF, AM, FM, and PM, and the corresponding H values are shown in Fig. 3. On the one hand, both of SPWV and STFT have larger H values than the proposed RTFA, which stem from the artifacts arising from the crossing terms of SPWV and the low TF resolution of STFT, respectively. In other words, the drawbacks of SPWV and STFT may add false TF components to the TF spectrum, and thus the H value may become large, suggesting the low accuracy of signal-level evaluation. On the other hand, since we have argued that the four types of blanket jamming have similar approximate statistics to complex Gaussian noise, it is desirable to have similar H values, when they have the same SJR. As shown in Fig. 3, the proposed RTFA has the smallest variation of H, which is consistent to the theoretical analysis. In the sequel, the proposed RTFA can exactly and robustly provide TF spectrum for the subsequent evaluation.

B. PAPR

On PAPR, we mainly consider its variation as SJR varies in this subsection, and its relationship with CFAR detection will be demonstrated in next subsection. For clarity, we assume there is only one target and its radical range, radical velocity and RCS are 10km, -200m/s and 1m^2, respectively, where the negativeness of velocity means the target is moving towards the radar. Echoes of the target in jamming-free environment and the results of matched filtering and MTD are shown in Fig. 4, all of which are consistent to the theoretical models. For example, the LFM signals are compressed at the location of 10km (see Fig. 4b) by matched filtering and the Doppler frequency estimated by MTD (shown in Fig. 4c) also equals to that computed by $f_d = -2vf_0/c = 4/3 \times 10^3$Hz.

When we add the RF jamming with SJR of -20dB to the echoes, the corresponding results are presented in Fig. 5. It can be observed in Fig. 5a that the RF jamming is so strong that the LFM waveform of the target has been suppressed significantly. A faint range line, however, can be also checked

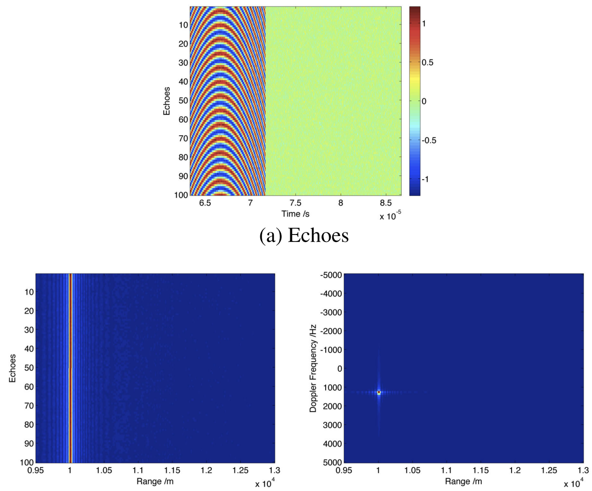

(a) Echoes

(b) Result of matched filtering

(c) Result of MTD

FIGURE 4. Echoes of the target in jamming-free environment and the results of matched filtering and MTD.

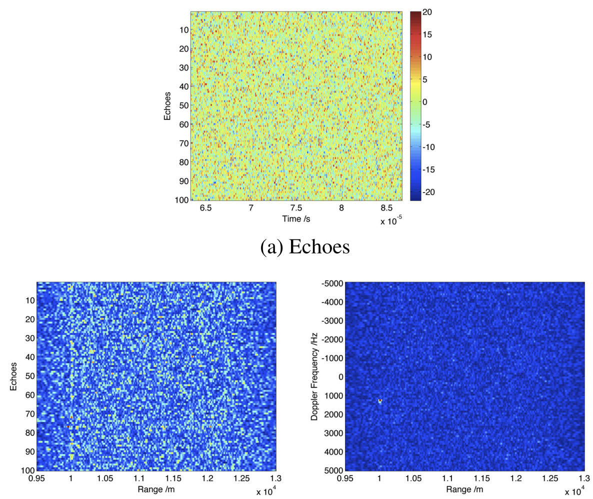

(a) Echoes

(b) Result of matched filtering

(c) Result of MTD

FIGURE 5. Echoes of the target in RF jamming environment (SJR: -20dB) and the results of matched filtering and MTD.

at the location of 10km in Fig. 5b, depending on the improvement of SJR by matched filtering. In fact, the SJR can be further improved by MTD as it is clear to see the target on the range dimension of 10km and the frequency dimension of $4/3 \times 10^3$Hz in Fig. 5c. Thus, the comparison between Fig. 4 and Fig. 5 can visually validate the function of matched filtering and MTD on SJR.

In order to quantitatively demonstrate the results in Theorem 2, we present the PAPR curves with respect to SJR for blanket jamming in Fig. 6, where the SJR is uniformly set from -40dB to 30dB, with the gap of 5dB. Fig. 6 implies two similarities and the first one is that the PAPR curves for blanket jamming have high consistency to the theoretical curve determined by Theorem 2. According to the theoretical curve, when the SJR is less than some thresholding, all of

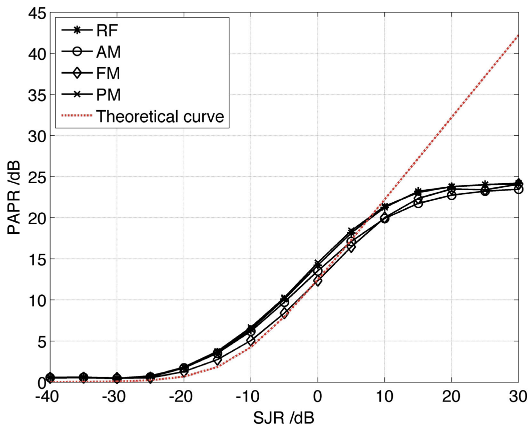

FIGURE 6. PAPR curves for blanket jamming.

TABLE 2. Weighting coefficients and normalization factors for composite evaluation.

w_H	w_μ	$\frac{w_H}{w_H+w_\mu}$	$\frac{w_\mu}{w_H+w_\mu}$	$H_{\max}$	$H_{\min}$	$\mu_{\max}$	$\mu_{\min}$
0.26	0.71	0.27	0.73	3.70	1.59	24.11	0.39

the PAPR curves are nearly zero; otherwise, it is desirable to approximately fit them by a linear function. However, there exists an inflection point at the SJR of around 20dB, which arises from the fact that the noise added to radar with SNR of 20dB begins to limit the further increase of PAPR when the SJR increases to around 20dB. Another similarity refers to the consistency among the PAPR curves for the four types of blanket jamming, not only indirectly validating the approximate statistics of blanket jamming in PD radar, but also providing the basis for the unified evaluation framework.

C. COMPOSITE EVALUATION

The numerical experiments in the two subsections above have illustrated the superiorities of the proposed RTFA and the accuracy of the Theorem 2 for PAPR, respectively, and now we focus on the performance of composite evaluation, which can also validate Theorem 3 for PAPR indirectly. In the following, we first present the samples to estimate the normalization factors and weighting coefficients for composite evaluation, and then the evaluation results with respect to different SJR values are listed to validate the feasibility of composite evaluation.

For sample set $\{J_{mn}^k | m = 1, 2, \cdots, M; n = 1, 2, \cdots, N; k = 1, 2, 3, 4.\}$, the SJR values are set uniformly from -30dB to 30dB, with the gap of 3dB, and so $M = 21$ and there are $4M = 84$ jamming property labels. For robustness, we also set the number of samples as $N = 100$ for each jamming property label, and thus there are 8400 samples in total. From the sample set, the composition parameters are estimated and shown in table 2, from which we can see that the weighting coefficient for μ is bigger than that for H and that the index μ of the sample set is also within a larger range than the index H.

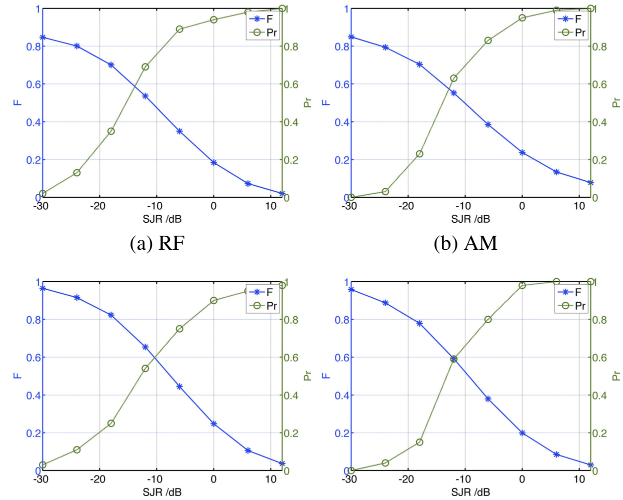

(a) RF (b) AM (c) FM (d) PM

FIGURE 7. Composite evaluation index F and CFAR detection probability P_r for different jamming types and different SJR values.

Following the related parameters above, we can calculate the composite evaluation index F for four types of blanket jamming under different SJR values and the results are shown in Fig. 7. Meanwhile, CFAR detection is used to assess the feasibility of composite evaluation, and thus we also plot the corresponding detection probability P_r in Fig. 7. We have to mention that the cell average approach [36] is used for CFAR detection and the false alarm probability is set as $P_{fa} = 0.001$. Moreover, to measure the consistency between F and P_r, we introduce the correlation coefficient:

$$\eta = \frac{\mathrm{cov}(F, P_r)}{\sigma_F \sigma_{P_r}} \tag{41}$$

where $\mathrm{cov}(F, P_r)$ is the covariance between F and P_r and σ is the standard deviation. From the definition above, we have $\eta \in [-1, 1]$. When the jamming intensity increases, it is expected that the composite index F also increases but the detection probability decreases, implying that η approaches to -1. In fact, we can observe these trends from the curves in Fig. 7. Also, the correlation coefficients between F and P_r in Fig. 8 tell that the composite evaluation has high consistent to CFAR detection, since all of them approach to -1.

We have argued that the performance of composite evaluation can validate the relationship between SJR and detection probability, which can also support Theorem 3 indirectly. As stated in Theorem 2, when the jamming power is small enough, the SJR will be significantly big and it approximately holds that $\mu \approx \mathrm{SJR} + C$ with constant C; otherwise, $\mu \approx 0$. In the former case, we can derive that $P_r = (P_{fa})^{10^{-\mu/10}} \approx 1$ as SJR increases; while, in the later case, we have $P_r = P_{fa} = 0.001 \approx 0$. This analysis is consistent to Fig. 7, which validates the quantitative relationship between SJR and detection probability as well as the main results in Theorem 3.

In the end, we aim to give some remarks on the numerical experiments. First of all, the composite evaluation combines

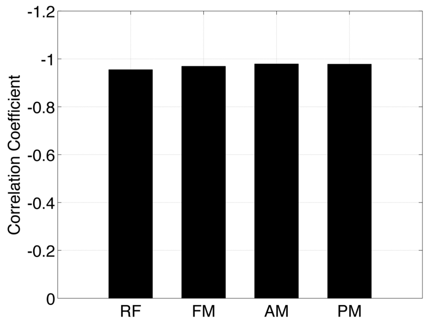

FIGURE 8. Correlation coefficients between F and P_r for blanket jamming.

the signal-level evaluation and the system/application-level evaluation together, so it is feasible and robust for evaluating the effect of jamming on radar via associating their advantages. Meanwhile, the composite evaluation provides a unified evaluation framework for four types of blanket jamming and PD radar with multiple tasks, since the approximate statistics of blanket jamming is analyzed and the CFAR detection is viewed as one of the most foundational application for PD radar. Finally, it is possible to further improve the estimation accuracy of normalization factors and weighting coefficients, when the sample set is enlarged.

VII. CONCLUSION

To tackle the restrictions from diverse jamming types and radar's applications, we put forward a unified framework for evaluating the effect of blanket jamming on radar by combining RTFA and PAPR. On the one hand, the modified RTFA is developed to improve the TF resolution and accuracy and to avoid the artifacts for TF spectrum, allowing us to implement an accurate signal-level evaluation via 2D image entropy. On the other hand, the quantitative relationship between the SJR of echoes and the detection probability of CFAR detection is achieved by the PAPR, and thus the jamming mechanism is uncovered partly and the system/application-level evaluation also has the theoretical guarantee. To composite the elevation indices above, we exploit normalization and weighted averaging using composite parameters estimated from the sample set, enhancing the robustness and the data-driven property of composite evaluation. In numerical experiments, the superiority of the proposed RTFA and the main results for PRAR have been validated by comparing with traditional TF analysis methods and by analyzing the PAPR and detection probability under different SJR values, respectively. More importantly, the feasibility of composite evaluation, including the estimation of composite parameters and the consistency to CFAR detection, is also illustrated by four types of blanket jamming.

The future extension of this work can be summarized in the following three aspects. In term of theory, the convolution framelets for RTFA can be further designed or trained to improve its representation ability and the radar system constants in Theorem 2 can be further determined to develop a more accurate result. In the aspect of method, the composite evaluation associates with the signal-level evaluation and the system/application-level evaluation together, however, it is also possible to combine more evaluations from the middle processing steps besides that from both ends of head and tail. Finally, the proposed evaluation method can be extended and applied to other jamming cases, such as the deception jamming (e.g. false targets and velocity deception) and radars with other tasks (e.g. tracking, imaging and recognition).

APPENDIX

Proof of Lemma 2: Starting from the orthogonality of $\mathbf{U}$ and $\mathbf{V}$, we can conclude that $\{\mathbf{u}_i\mathbf{v}_j^T | i = 1, 2, \cdots N, j = 1, 2 \cdots, M\}$ can be regarded as the orthogonal bases of $\mathbb{R}^{N\times M}$ equipped with inner product $< \mathbf{A}, \mathbf{B} >= \mathrm{Tr}(\mathbf{A}\mathbf{B}^T)$, where $\mathbf{A}, \mathbf{B} \in \mathbb{R}^{N\times M}$ and $\mathrm{Tr}(\cdot)$ is the trace of a matrix. In other words, for $\mathbf{X} \in \mathbb{R}^{N\times M}$. it can be linearly represented by the orthogonal bases, namely

$$\begin{aligned}\mathbf{X} &= \sum_{i=1}^{N}\sum_{j=1}^{M} < \mathbf{X}, \mathbf{u}_i\mathbf{v}_j^T > \mathbf{u}_i\mathbf{v}_j^T \\ &\triangleq \sum_{i=1}^{N}\sum_{j=1}^{M} \mathbf{\Gamma}_{ij}\mathbf{u}_i\mathbf{v}_j^T \\ &= \mathbf{U}\mathbf{\Gamma}\mathbf{V}^T,\end{aligned}$$

where $\mathbf{\Gamma}_{ij} =< \mathbf{X}, \mathbf{u}_i\mathbf{v}_j^T >= \mathrm{Tr}(\mathbf{X}\mathbf{v}_j\mathbf{u}_i^T) = \mathbf{u}_i^T\mathbf{X}\mathbf{v}_j$. Notice lemma 1 tells that the Hankel matrix satisfies

$$\mathbf{u}_i^T(\mathbf{X}\mathbf{v}_j) = \mathbf{u}_i^T(\mathbf{x} \circledast \mathbf{v}_j^-) = \mathbf{x}^T(\mathbf{u}_i \circledast \mathbf{v}_j),$$

so we have $\mathbf{\Gamma}_{ij} = \mathbf{x}^T(\mathbf{u}_i \circledast \mathbf{v}_j)$ and the first statement is achieved.

It is also worth noting that the quantitative relationship between $\mathbf{x}$ and $\mathbf{X}$ has been given by the first conclusion in Lemma 1, and thus $\mathbf{x}$ has the linear representation of the form

$$\begin{aligned}\mathbf{x} &= \frac{1}{N}\sum_{i=1}^{N}\sum_{j=1}^{M} < \mathbf{x}, \mathbf{u}_i \circledast \mathbf{v}_j > \mathbf{u}_i \circledast \mathbf{v}_j \\ &= \frac{1}{N}\sum_{i=1}^{N}\sum_{j=1}^{M} \mathbf{\Gamma}_{ij}\mathbf{u}_i \circledast \mathbf{v}_j,\end{aligned}$$

which means the second statement holds for $\mathbf{x}$. Thus the proof is completed. ■

Proof of Theorem 1: In light of the complex formats of $\mathbf{x} \in \mathbb{C}^M$ and its Hankel matrix $\mathbf{X} \in \mathbb{C}^{N\times M}$, they can be decomposed into $\mathbf{x} = \mathbf{x}_1 + j_0\mathbf{x}_2$ and $\mathbf{X} = \mathbf{X}_1 + j_0\mathbf{X}_2$, respectively, where $\mathbf{x}_1, \mathbf{x}_2 \in \mathbb{R}^M$, $\mathbf{X}_1, \mathbf{X}_2 \in \mathbb{R}^{N\times M}$, and $j_0 = \sqrt{-1}$. With orthogonal matrices $\mathbf{\Phi}$ and $\mathbf{E}$ in Theorem 1, Lemma 2 and Lemma 3 tell that the representation

$$\begin{cases}\mathbf{X}_1 = \mathbf{\Phi}\mathbf{C}_1\mathbf{E} \\ \mathbf{X}_2 = \mathbf{\Phi}\mathbf{C}_2\mathbf{E}\end{cases}$$

and

$$\begin{cases} \mathbf{x}_1 = \frac{1}{N}\sum_{i=1}^{N}\sum_{j=1}^{M}(\mathbf{C}_1)_{ij}\boldsymbol{\phi}_i \circledast \mathbf{e}_j \\ \mathbf{x}_2 = \frac{1}{N}\sum_{i=1}^{N}\sum_{j=1}^{M}(\mathbf{C}_2)_{ij}\boldsymbol{\phi}_i \circledast \mathbf{e}_j \end{cases}$$

holds for the convolution framelets $\{\boldsymbol{\phi}_i \circledast \mathbf{e}_j | i = 1, 2\cdots, N, j = 1, 2, \cdots, M\}$ constructed from $\boldsymbol{\Phi}$ and $\mathbf{E}$. In this case, $\mathbf{x}$ and $\mathbf{X}$ have the decomposition

$$\begin{aligned} \mathbf{x} &= \mathbf{x}_1 + j_0\mathbf{x}_2 \\ &= \frac{1}{N}\sum_{i=1}^{N}\sum_{j=1}^{M}[(\mathbf{C}_1)_{ij} + j_0(\mathbf{C}_2)_{ij}]\boldsymbol{\phi}_i \circledast \mathbf{e}_j \\ &\triangleq \frac{1}{N}\sum_{i=1}^{N}\sum_{j=1}^{M}\mathbf{C}_{ij}\boldsymbol{\phi}_i \circledast \mathbf{e}_j \end{aligned}$$

and

$$\mathbf{X} = \mathbf{X}_1 + j_0\mathbf{X}_2 = \boldsymbol{\Phi}(\mathbf{C}_1 + j_0\mathbf{C}_2)E = \boldsymbol{\Phi}\mathbf{C}\mathbf{E} = \boldsymbol{\Phi}\mathbf{C},$$

respectively.

If $\mathbf{X} = \boldsymbol{\Phi}\mathbf{S}$, $\mathbf{S} = \mathbf{C}$ also holds for the orthogonality of $\boldsymbol{\Phi}$ and thus we have the linear representation

$$\mathbf{x} = \frac{1}{N}\sum_{i=1}^{N}\sum_{j=1}^{M}\mathbf{S}_{ij}\boldsymbol{\phi}_i \circledast \mathbf{e}_j \triangleq \boldsymbol{\Sigma}\mathbf{s},$$

where $\mathbf{s}$ the vectorization of $\mathbf{S}$ and $\boldsymbol{\Sigma}$ is the convolution framelets constructed from $\boldsymbol{\Phi}$ and $\mathbf{E}$. So the proof is completed. ■

Proof of Lemma 5: As we have argued in the proof of Lemma 4, $\mathrm{SJR}_1 = 10\log_{10}(P_s^1/P_J^1)$ holds at r_0 for each echo, where P_s^1 is actually the energy of LFM signal. On the one hand, $s_1(t_m, r)$ in (27) at $r = r_0$ can be rewritten as

$$s_1(t_m, r_0) = C_1\exp(-j2\pi f_d t_m) \triangleq s_1(t_m)$$

On the other hand, J_1 satisfies complex Gaussian distribution, so the average power P_J^2 of J_2 in (28) can be derived by

$$P_J^2 = P_J^1 \cdot \int_0^{T_a} |\exp(-j2\pi f t_m)|^2 dt_m = P_J^1 \cdot T_a$$

As a result, the power ratio between the true signal and the jamming after MTD, at $r = r_0$, can be expressed as

$$\frac{P_s^2}{P_J^2} = \frac{|\int_0^{T_a} s_1(t_m)\exp(-j2\pi f t_m)dt_m|^2}{P_J^1 \cdot T_a}$$

Schwarz inequality tells that the power ratio above would reach maximum, if $s_1(t_m) = k\exp(j2\pi f t_m)$ (suggesting $f = -f_d$) holds for constant k. Thus at $(-f_d, r_0)$ we have

$$\frac{P_s^2}{P_J^2} = \frac{\int_0^{T_a}|s_1(t_m)|^2 dt_m}{P_J^1}$$

Notice that the energy of $s_1(t_m, r_0)$ at $r = r_0$ (i.e., $s_1(t_m)$) is the power P_s^1, so the integration of $s_1(t_m)$ can be computed by

$$\int_0^{T_a}|s_1(t_m)|^2 dt_m = k_a N_a \cdot P_s^1$$

where k_a is a radar system constant. Therefore, the SJR value of x_2 at $(-f_d, r_0)$ is

$$\mathrm{SJR}_2 = 10\log_{10}\left(\frac{P_s^2}{P_J^2}\right) = 10\log_{10}\left(\frac{k_a N_a \cdot P_s^1}{P_J^1}\right)$$

Thus we have $\mathrm{SJR}_2 = \mathrm{SJR}_1 + 10\log_{10}(k_a N_a)$ and the proof is completed. ■

REFERENCES

[1] L. Jianxun, L. Weidong, and L. Guisheng, "Efficiency assessment of general radar under jamming," *J. Xidian Univ.*, vol. 27, no. 4, pp. 520–523, 2000.

[2] S. Mighani, M. Mivehchy, and M. F. Sabahi, "Evaluating sweep noisy barrage jamming effect on tracking radar based on functioning destruction time," in *Proc. 7th Int. Symp. Telecommun. (IST)*, Tehran, Iran, Sep. 2014, pp. 400–404.

[3] E. Mintzias, R. A. Romero, and T. Ha, "Performance evaluation of complex spreading MIMO systems in Rayleigh fading and interference," in *Proc. Int. Waveform Diversity Design Conf. (WDD)*, Kauai, HI, USA, Jan. 2012, pp. 97–102.

[4] L. Yuan and L. Dashe, "A quick and unitary algorithm for imaging radar jamming effect evaluation," in *Proc. IEEE 10th Int. Conf. SIGNAL Process. Proc.*, Beijing, China, Oct. 2010, pp. 2328–2331.

[5] J.-W. Xu, L. Gui-Sheng, and Z. Yu-Hong, "On anti-jamming technique with waveform diverse array radar," *Acta Electronica Sinica*, vol. 27, no. 3, pp. 545–551, 2019.

[6] M. Ren, G. Yan, Y. Zhu, Z. Wang, and T. Gao, "Study on radar anti-jamming performance test method in complex electromagnetic environment," *Chin. J. Sci. Instrum.*, vol. 34, no. 6, pp. 1277–1282, 2016.

[7] S. Paine, D. W. O'Hagan, M. Inggs, C. Schupbach, and U. Boniger, "Evaluating the performance of FM-based PCL radar in the presence of jamming," *IEEE Trans. Aerosp. Electron. Syst.*, vol. 55, no. 2, pp. 631–643, Apr. 2019.

[8] S. You, M. Diao, and L. Gao, "Implementation of a combinatorial-optimisation-based threat evaluation and jamming allocation system," *IET Radar, Sonar Navigat.*, vol. 13, no. 10, pp. 1636–1645, Oct. 2019.

[9] L. M. Surhone, T. M. Timpledon, and S. F. Marseken, *Radar Jamming and Deception*. Helena, MT, USA: Betascript, 2010.

[10] X. Liu and D. Li, "Analysis of cooperative jamming against pulse compression radar based on CFAR," *EURASIP J. Adv. Signal Process.*, vol. 2018, no. 1, pp. 1–12, Dec. 2018.

[11] D. Huang, G. Cui, X. Yu, M. Ge, and L. Kong, "Joint range–velocity deception jamming suppression for SIMO radar," *IET Radar, Sonar Navigat.*, vol. 13, no. 1, pp. 113–122, Jan. 2019.

[12] J. DiFranco and C. Kaiteris, "Radar performance review in clear and jamming environments," *IEEE Trans. Aerosp. Electron. Syst.*, vol. AES-17, no. 5, pp. 701–710, Sep. 1981.

[13] D. Adamy, "Radar jamming techniques," *J. Electron. Defense*, vol. 33, no. 1, pp. 44–46, 2010.

[14] W. Liu, J. Meng, and L. Zhou, "Impact analysis of DRFM-based active jamming to radar detection efficiency," in *Proc. IET Int. Radar Conf.*, Nanjing, China, 2018, pp. 1–3.

[15] C. Alabaster, *Pulse Doppler Radar: Principles, Technology, Applications*. Raleigh, NC, USA: SciTech Publishing, 2012.

[16] X. Shi, F. Zhou, X. Bai, and H. Su, "Deceptive jamming for tracked vehicles based on micro-Doppler signatures," *IET Radar, Sonar Navigat.*, vol. 12, no. 8, pp. 844–852, Aug. 2018.

[17] H. Hao, D. Zeng, and P. Ge, "Research on the method of smart noise jamming on pulse radar," in *Proc. 5th Int. Conf. Instrum. Meas., Comput., Commun. Control (IMCCC)*, Qinhuangdao, China, Sep. 2015, pp. 1339–1342.

[18] T. Li, Z. Wang, and J. Liu, "Evaluation method for impact of jamming on radar based on expert knowledge and data mining," *IET Radar, Sonar Navigat.*, vol. 14, no. 9, pp. 1441–1450, Sep. 2020.

[19] X. Tian and B. Tang, "Spectrum texture features based radar deception jamming recognition using joint frequency-slow time processing," *J. Comput. Inf. Syst.*, vol. 9, no. 13, pp. 5181–5188, 2013.

[20] D. X. Sun, G. H. Wang, and D. Sheng, "Technique for multi-range-false target jamming identification based on statistical characteristic discrepancy," *Syst. Eng. Electron.*, vol. 39, no. 4, pp. 748–757, May 2017.

[21] M. Zhu, Y. Li, Z. Pan, and J. Yang, "Automatic modulation recognition of compound signals using a deep multi-label classifier: A case study with radar jamming signals," *Signal Process.*, vol. 169, pp. 1–13, Apr. 2020.

[22] X. Tian, B. Tang, and G. Gui, "Product spectrum matrix feature extraction and recognition of radar deception jamming," *Int. J. Electron.*, vol. 100, no. 12, pp. 1621–1629, Dec. 2013.

[23] A. Soto, A. Mendoza, and B. C. Flores, "Optimization of neural network architecture for classification of radar jamming FM signals," *Radar Sensor Technol. XXI*, vol. 10188, pp. 1–11, May 2017.

[24] J. S. Patel, F. Fioranelli, M. Ritchie, and H. D. Griffiths, "Fusion of deep representations in multistatic radar networks to counteract the presence of synthetic jamming," *IEEE Sensors J.*, vol. 19, no. 15, pp. 6362–6370, Aug. 2019.

[25] P. Gao *et al.*, "GNSS spoofing jamming recognition based on machine learning," in *Proc. Int. Conf. Signal Inf. Process., Netw. Comput.*, Chongqi, China, 2017, pp. 221–228.

[26] H. Azami, L. E. V. da Silva, A. C. M. Omoto, and A. Humeau-Heurtier, "Two-dimensional dispersion entropy: An information-theoretic method for irregularity analysis of images," *Signal Process., Image Commun.*, vol. 75, pp. 178–187, Jul. 2019.

[27] L. Zunino and H. V. Ribeiro, "Discriminating image textures with the multiscale two-dimensional complexity-entropy causality plane," *Chaos, Solitons Fractals*, vol. 91, pp. 679–688, Oct. 2016.

[28] S. Zhang and Y. D. Zhang, "Robust time–frequency analysis of multiple FM signals with burst missing samples," *IEEE Signal Process. Lett.*, vol. 26, no. 8, pp. 1172–1176, Aug. 2019.

[29] S. Liu, Y. D. Zhang, T. Shan, and R. Tao, "Structure-aware Bayesian compressive sensing for frequency-hopping spectrum estimation with missing observations," *IEEE Trans. Signal Process.*, vol. 66, no. 8, pp. 2153–2166, Apr. 2018.

[30] L. Stankovic, S. Stankovic, I. Orovic, and M. G. Amin, "Robust time-frequency analysis based on the L-Estimation and compressive sensing," *IEEE Signal Process. Lett.*, vol. 20, no. 5, pp. 499–502, May 2013.

[31] L. Liu and G. Q. Zhao, "A method on peak-to-average power ratio reduction," *Acta Electronica Sinica*, vol. 46, no. 10, pp. 2443–2449, 2018.

[32] R. Yin, T. Gao, Y. M. Lu, and I. Daubechies, "A tale of two bases: Local-nonlocal regularization on image patches with convolution framelets," *SIAM J. Imag. Sci.*, vol. 10, no. 2, pp. 711–750, Jan. 2017.

[33] E. Crespo Marques, N. Maciel, L. Naviner, H. Cai, and J. Yang, "A review of sparse recovery algorithms," *IEEE Access*, vol. 7, pp. 1300–1322, 2019.

[34] E. D. Livshitz and V. N. Temlyakov, "Sparse approximation and recovery by greedy algorithms," *IEEE Trans. Inf. Theory*, vol. 60, no. 7, pp. 3989–4000, Jul. 2014.

[35] R. K. Mallik, "On multivariate Rayleigh and exponential distributions," *IEEE Trans. Inf. Theory*, vol. 49, no. 6, pp. 1499–1514, Jun. 2003.

[36] A. Zaimbashi, "An adaptive cell averaging-based CFAR detector for interfering targets and clutter-edge situations," *Digit. Signal Process.*, vol. 31, pp. 59–68, Aug. 2014.

TINGPENG LI received the B.S. degree in mechanical engineering from the National University of Defense Technology (NUDT), Changsha, China, in 2010, and the M.S. and Ph.D. degrees in mechanical engineering, in 2013 and 2016, respectively. His research interests include integration support technology and complex electromagnetic environment effects.

ZELONG WANG received the Ph.D. degree in system analysis and integration from the National University of Defense Technology, in 2013. He is currently an Associate Professor of data analysis with the National University of Defense Technology. His research interests include data mining and deep learning.

JIYING LIU received the Ph.D. degree in system analysis and integration from the National University of Defense Technology, in 2010. He is currently an Associate Professor of signal processing with the National University of Defense Technology. His research interests include radar imaging and data mining.